Biosensors and Bioelectronics 155 (2020) 112107

Contents lists available at ScienceDirect

Biosensors and Bioelectronics

journal homepage: http://www.elsevier.com/locate/bios

Self-partitioning SlipChip for slip-induced droplet formation and human papillomavirus viral load quantification with digital LAMP

Ziqing Yu [a,1], Weiyuan Lyu [a,1], Mengchao Yu [a,1], Qian Wang [b,c,d,1], Haijun Qu [a], Rustem F. Ismagilov [e,f], Xu Han [b,c,d], Dongmei Lai [b,c,d,**], Feng Shen [a,*]

[a] School of Biomedical Engineering, Shanghai Jiao Tong University, 1954 Huashan Road, Shanghai, 200030, China
[b] The International Peace Maternity and Child Health Hospital, School of Medicine, Shanghai Jiao Tong University, Shanghai, China
[c] Shanghai Key Laboratory of Embryo Original Diseases, Shanghai, China
[d] Shanghai Municipal Key Clinical Specialty, Shanghai, China
[e] Division of Chemistry & Chemical Engineering, California Institute of Technology, 1200 East California Boulevard, Mail Code 210-41, Pasadena, CA, 91125, United States
[f] Division of Biology & Biological Engineering, California Institute of Technology, 1200 East California Boulevard, Mail Code 210-41, Pasadena, CA, 91125, United States

ARTICLE INFO

Keywords:
Lab on a chip
Digital PCR
Droplet
Point-of-care
Microfluidics

ABSTRACT

Human papillomavirus (HPV) is one of the most common sexually transmitted infections worldwide, and persistent HPV infection can cause warts and even cancer. Nucleic acid analysis of HPV viral DNA can be very informative for the diagnosis and monitoring of HPV. Digital nucleic acid analysis, such as digital PCR and digital isothermal amplification, can provide sensitive detection and precise quantification of target nucleic acids, and its utility has been demonstrated in many biological research and medical diagnostic applications. A variety of methods have been developed for the generation of a large number of individual reaction partitions, a key requirement for digital nucleic acid analysis. However, an easily assembled and operated device for robust droplet formation without preprocessing devices, auxiliary instrumentation or control systems is still highly desired. In this paper, we present a self-partitioning SlipChip (sp-SlipChip) microfluidic device for the slip-induced generation of droplets to perform digital loop-mediated isothermal amplification (LAMP) for the detection and quantification of HPV DNA. In contrast to traditional SlipChip methods, which require the precise alignment of microfeatures, this sp-SlipChip utilized a design of "chain-of-pearls" continuous microfluidic channel that is independent of the overlapping of microfeatures on different plates to establish the fluidic path for reagent loading. Initiated by a simple slipping step, the aqueous solution can robustly self-partition into individual droplets by capillary pressure-driven flow. This advantage makes the sp-SlipChip very appealing for the point-of-care quantitative analysis of viral load. As a proof of concept, we performed digital LAMP on a sp-SlipChip to quantify human papillomaviruses (HPVs) 16 and 18 and tested this method with fifteen anonymous clinical samples.

1. Introduction

This paper describes a self-partitioning SlipChip (sp-SlipChip) microfluidic device for slip-induced droplet formation and its application in the viral load quantification of high-risk human papillomaviruses (HPV 16, 18), which are considered a necessary cause of human cervical cancer (De Martel et al., 2012; Muñoz et al., 2003), by digital loop-mediated isothermal amplification (LAMP). HPV is a global health burden, and persistent HPV infection can cause cervical cancer(Crow, 2012). Among the tens of different HPV types that can infect humans, HPV-16 and HPV-18 are estimated to account for approximately 70% of cervical cancer cases(Seoud et al., 2011). Although nucleic acid analysis for HPV have become available (Park et al., 2012), they are generally limited to clinical laboratories due to the workflow, instrumentation,

* Corresponding author.
** Corresponding author. The International Peace Maternity and Child Health Hospital, School of Medicine, Shanghai Jiao Tong University, Shanghai, China.
E-mail addresses: laidongmei@hotmail.com (D. Lai), feng.shen@sjtu.edu.cn (F. Shen).
[1] Z. Y., W. L., M. Y., and Q. W. contributed equally.

https://doi.org/10.1016/j.bios.2020.112107
Received 23 October 2019; Received in revised form 5 February 2020; Accepted 17 February 2020
Available online 18 February 2020

and personnel required. A nucleic acid test for HPV diagnosis and monitoring in a point-of-care setting is still highly desired.

Digital nucleic acid analysis (NAA), such as digital PCR and digital isothermal amplification, compartmentalizes solutions containing target nucleic acids into a large number of partitions, which can be grouped into "1"s and "0"s after nucleic acid amplification(Cao et al., 2016; Zhu and Wang, 2017). Poisson statistical analysis allows calculation of the target nucleic acid concentration(Kreutz et al., 2011). Digital NAA can provide precise quantification of target nucleic acids and has been demonstrated to tolerate inhibition from raw samples and environmental variation(Shen et al., 2011a; Zhang et al., 2015a). Digital NAA has been demonstrated in many biological research and medical diagnostic applications, including mutation analysis (Taly et al., 2013), epigenetic investigations (Wu et al., 2017), viral load quantification (Huang et al., 2015), the study of extracellular vesicles (Bai et al., 2019), and prenatal diagnosis(Lo et al., 2007).

A variety of microfluidics-based methods have been developed to generate a large number of small-volume reaction partitions to perform digital NAA. Different microwell and microchamber designs were developed to compartmentalize liquid in small volumes(Heyries et al., 2011; Kreutz et al., 2019; Ottesen et al., 2006; Zhou et al., 2019). Microfluidic devices with the features of co-flow, crossflow, and flow focusing were demonstrated to reliably form liquid droplets with high throughput(Hindson et al., 2011; Nie et al., 2019; Zeng et al., 2013; Zhang et al., 2015a). In addition, approaches with mechanical dispensing or agitation (Jiang et al., 2016; Zhu et al., 2015) and centrifugal force (Chen et al., 2017) have been demonstrated to form droplets with good uniformity and high throughput. Although many of these methods have demonstrated stable performance and good robustness, many of them still require preprocessing devices, auxiliary instrumentation or fluidic control systems.

SlipChips are a type of microfluidic device that can partition liquid by the relative movement of two microfluidic plates with imprinted microwells or fluidic ducts on the contacting surface(Cai et al., 2014; Du et al., 2009; Li et al., 2010; Liu et al., 2010; Shen et al., 2014, 2011b; 2010; Sun et al., 2013; Yu et al., 2019). They do not require additional auxiliary systems, such as pumps, pneumatic systems, and electronic systems, for control and manipulation of the liquid. However, these traditional SlipChips generally require the precise alignment of microwells or fluidic ducts on different plates to establish or break fluidic paths, which may limit their widespread application in different settings.

This paper reports our work towards developing an easily assembled and operated microfluidic device to perform digital NAA in on-demand settings. We present a surface tension-driven sp-SlipChip that can generate droplets by slip-induced flow without requiring the precise alignment of microfeatures. Whereas surface tension has been used previously to generate droplets on traditional SlipChips by carefully aligning one set of microwells over another (Du et al., 2009), which can be challenging in low-resource settings, we herein utilized a large, easily visible channel to induce droplet formation. The sp-SlipChip contains "chain-of-pearls" continuous fluidic channels that allow liquid to be introduced into the device. With one simple manual slipping step, the chain-of-pearls channel can overlap with the expansion channel on the other device plate. Surface tension drives the liquid to break at the "neck" and form individual droplets. This slip-induced self-partitioning process is regulated by the physical geometry of the "chain-of-pearls" channel and the surface properties instead of by micro-alignment; therefore, this process is generally very robust and provides reproducible droplet formation.

As a proof of concept, we applied this sp-SlipChip to the quantification of HPV viral load by digital LAMP. The sp-SlipChip can generate a large number of partitions, which are required for digital NAA, with simple alignment and operation steps. Here, we demonstrated a sp-SlipChip device for the quantification of HPV load with digital LAMP and tested the device with nucleic acids extracted from fifteen anonymous clinical cervical swab samples. Furthermore, droplets of different sizes and components generated from the sp-SlipChip can provide desired physical and chemical properties and a controlled microenvironment for potential additional physical, chemical, biological, and medical applications, including protein crystallization, NAA, immunoassays, and single-cell investigations.

2. Material and methods

2.1. Fabrication of the SlipChip device

The chip patterns were designed in AutoCAD (Autodesk, San Rafael, CA, USA) and printed onto photomasks (MICROCAD PHOTO-MASK LTD, Shenzhen, China). The sp-SlipChip was composed of two layers of glass plates. The top plate contained fluidic inlets and straight expansion channels, and the bottom plate contained continuous "chain-of-pearls" shaped microfluidic channels.

For the top plate, the soda-lime glass plate coated with chromium and photoresist was aligned with the photomask with straight expansion channels and then exposed to UV light in a UV flood curing system for 12 s. Then, the exposed glass plate was immersed in 0.1 mol L^{-1} NaOH solution for 60 s to remove the reacted photoresist. Next, the glass plate was submerged in a chromium etchant solution described previously(Yu et al., 2019). The glass etching was conducted at 40 °C in a shaking water bath (frequency: 50 rpm/min). A profilometer (Bruker, Billerica, MA) was used to monitor the etching depth.

A two-step etching method was used to fabricate the bottom plate. First, the soda-lime glass plate (Fig. S1A) was aligned to the photomask with the "pearls" shape and exposed to UV light for 10 s (Fig. S1B). Then, NaOH solution and chromium etchant solution were used in sequence to remove the reacted photoresist and exposed chromium (Figs. S1C–S1D). After thorough rinsing with water and drying in air, the glass was aligned to the second film photomask with a "chain" shape and exposed to UV light for another 10 s (Fig. S1E). Then, NaOH solution was used to remove the reacted photoresist (Fig. S1F). The glass plate was then immersed in the glass etchant solution. The exposed glass with a "pearl" shape was etched to a desired depth (Fig. S1G). Then, the chromium etchant solution was used to remove the exposed chromium on the glass with a "chain" shape (Fig. S1H). Finally, the "chain-of-pearls" was etched to the desired depth (Fig. S1I).

After etching, the two glass plates were rinsed with water and placed in EtOH for 1 min to remove the remaining photoresist (Fig. S1J). Then, the glass plates were rinsed with water and submerged in chromium etchant solution to remove the remaining chromium layer (Fig. S1K). Prior to use, the surface of SlipChips was silanized with dimethyldichlorosilane by gas phase salinization for 1 h and then thoroughly cleaned with chloroform, acetone, and ethanol.

2.2. Measurement of droplet size distribution

A solution containing 1 mg mL^{-1} fluorescein and 10% food dye was loaded into the device. Then, the fluorescence signal was measured with Nikon Ti2 fluorescence microscope software (NIS-ElementsS-7 ver. 5.01).

2.3. Standard panels and clinical samples

The inserted fragment was PCR-amplified from HPV-16-positive serum using the HPV16–F3 and HPV16–B3 primers. Then, the DNA fragment was cloned into *Escherichia coli* DH5a cells using the PESI-T Vector System. The AxyPrep Plasmid Miniprep Kit was used to extract the recombinant plasmid. The DNA plasmid concentration was determined using a NanoDrop 1000 spectrophotometer (NanoDrop Technologies, Wilmington, DE). Swab samples of fifteen anonymous patients were obtained from The International Peace Maternity and Child Health Hospital. Genomic DNA was isolated with the QIAamp DNA Mini Kit.

2.4. LAMP reaction

The primers for HPV-16 and HPV-18 used in the paper were reported previously (Table S1). (Luo et al., 2011) A 25 μL LAMP reaction consisted of 1.6 μM each of the forward inner primer (FIP) and the backward inner primer (BIP), 0.8 μM each of the forward loop primer (LF) and the backward loop primer (BF), 0.2 μM each of the forward outer primer (F3) and the backward outer primer (B3), 2.5 μL of 10 × Isothermal Amplification Buffer, 6 mM $MgSO_4$, 8 U of *bst* DNA polymerase, 1.4 mM each of the dNTPs, 1 mg mL^{-1} BSA, 20 nM calcein, 0.4 mM $MnCl_2$ and 0.25 mM betaine. Five microliters of the template was added to the mixture, and the reaction was conducted at 65 °C for 60 min in an *in situ* thermal cycler (BIO-GENER, China).

2.5. Digital LAMP on sp-SlipChip

The aqueous solution containing LAMP reagents was introduced into the sp-SlipChip through the continuous chain-of-pearls-shaped microfluidic channels. After a simple slipping step, the chain-of-pearls-shaped microfluidic channels overlapped with the expansion channels, and the aqueous solution self-partitioned into individual droplets. Then, the device was placed on a thermal cycler (Eastwin Scientific Equipment Inc., Suzhou, China) with a customized *in situ* adaptor and incubated at 63 °C for 1 h.

Before and after thermal incubation, all chips were scanned on a Nikon Ti2 fluorescence microscope. It took approximately 10 min to scan the entire device. The images were automatically stitched together, and the average well intensity of the digital LAMP on the sp-SlipChip device was measured by using Nikon Ti2 fluorescence microscope software (NIS-Elements ver. 5.01) (Fig. S2). The cut-off value was defined as reported previously(Kreutz et al., 2019). The calculation of copy numbers based on the Poisson statistics was described previously (Shen et al., 2010). For all digital LAMP experiments, if there were fewer than three positive wells per device, then the experiments were determined to be negative.

2.6. Comparison of traditional SlipChip and sp-SlipChip

The traditional SlipChip requires good alignment of microfeatures on the top plate and the bottom plate. The partially overlapping area bridges two adjacent microwells. Any misalignment of the two plates could significantly change the overlapping area and affect proper reagent loading (Fig. S3A). The sp-SlipChip utilizes a "chain-of-pearls" continuous fluidic channel and slip-induced self-partitioning process to generate aqueous droplets. The misalignment of two microfluidic plates will not change the reagent loading and device operation process (Fig. S3B). Therefore, the sp-SlipChip could potentially provide a more robust and reproducible means to generate droplets than the traditional SlipChip.

3. Results and discussion

The sp-SlipChip device generates droplets based on a slip-induced self-partitioning effect driven by surface tension. This sp-SlipChip is composed of two microfluidic plates in close contact. The plates were fabricated from glass material with a wet etching method, and the surface of the device was silanized to make it hydrophobic (see Supporting Information for details). The top plate contains fluidic inlets and straight expansion channels (Fig. 1A); the bottom plate contains continuous chain-of-pearls-shaped microfluidic channels, where circular microwell "pearls" are connected by a shallow and narrow "chain" channel (Fig. 1B). A thin layer of lubricating oil was placed between the two plates to reduce slipping friction and to prevent the nonspecific adsorption of biomolecules to the surface. The two plates can be held in close contact by clamping fixtures without requiring partial overlap of the microfeatures on the top and bottom plates (Fig. 1C, F). At the initial loading position, aqueous fluid can be introduced into the chain-of-pearls channels by pipetting (Fig. 1D, G). Then, the top plate can be manually moved down relative to the bottom plate or controlled by a slipping gauge to bring the expansion channel into contact with the chain-of-pearls channel. Due to the difference in capillary pressure, the aqueous fluid breaks at the neck section of the chain channel and self-partitions into a spherical droplet surrounded by a lubricating oil phase (Fig. 1E, H).

The droplet formation by self-partitioning in the sp-SlipChip device is controlled by the capillary pressure. The surface of the sp-SlipChip is hydrophobic, and the gap and channels were initially occupied by lubricating oil, which can wet the surface but is immiscible with the aqueous solution. The capillary pressure, ΔP_{cap} [Pa], at the liquid-liquid interface along the microfluidic channel is determined by the geometry of the channel, such as width w_i [m] and height h_i [m] for a rectangular channel, the liquid-liquid interfacial tension γ [N/m], and the contact angle Θ [rad]. Calculating this value for a channel with a rectangular cross-section was described previously by equation (1)(Pompano et al., 2012):

$$\Delta P_{capi} = \left(\frac{2(w_i + h_i)}{w_i h_i}\right)\gamma \cos\theta = 2\left(\frac{1}{w_i} + \frac{1}{h_i}\right)\gamma \cos\theta \quad (1)$$

After the chain-of-pearls channel is completely filled with aqueous solution, γ is determined by the lubricating immiscible oil and aqueous

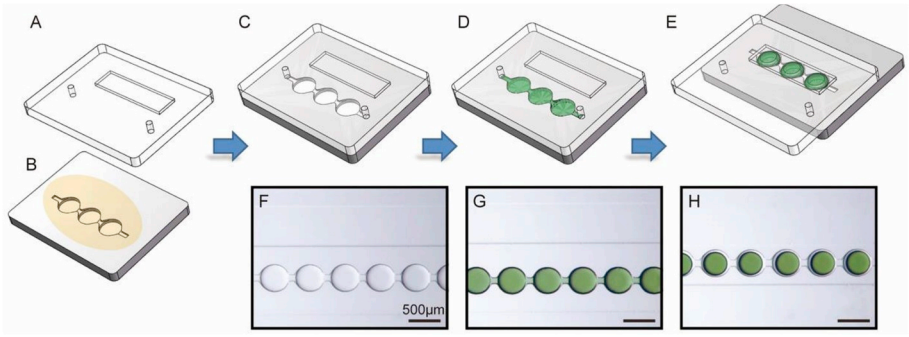

Fig. 1. Self-partitioning SlipChip for slip-induced droplet formation. (A) The top plate contains an extension channel, a fluidic inlet, and a fluidic outlet. (B) The bottom plate consists of a chain-of-pearls fluidic channel and lubricating oil (yellow). (C) The top and bottom plates are assembled in the initial loading position. (D) Aqueous solution (green) is introduced into the chain-of-pearls channel by pipetting. (E) The top plate is moved relative to the bottom plate to bring the chain-of-pearls channel into contact with the expansion channel by a manual slipping motion, and the aqueous solution self-partitions into individual droplets. (F) A zoomed-in bright-field photo of the device at the initial loading position. (G) A zoomed-in bright-field photo of the device loaded with aqueous solution containing green dye. (H) A zoomed-in bright-field photo of the device demonstrating the formation of individual droplets after the manual slipping step. (For interpretation of the references to colour in this figure legend, the reader is referred to the Web version of this article.)

solution, and Θ is determined by the properties of the lubricating immiscible oil, aqueous solution, and surface of the solid substrate. Before slipping occurs, the depth of the circular microwell, or the "pearl", is d_1 [m], and the radius is R [m]; for the microchannel that connects the microwell, or the neck of the "chain" section, the depth is d_2 [m], and the radius is w [m] (Fig. 2A). Therefore, the capillary pressure at the pearl, $\Delta P_{cap\ (pearl)}$, and at the chain section, $\Delta P_{cap\ (chain)}$, can be described as follows:

$$\Delta P_{cap(pearl)} \sim \left(\frac{1}{R}+\frac{1}{d_1}\right)\gamma\ \cos\theta \tag{2}$$

$$\Delta P_{cap(chain)} \sim \left(\frac{1}{w}+\frac{1}{d_2}\right)\gamma\cos\theta \tag{3}$$

In the design of the sp-SlipChip, R > w, and $d_1 > d_2$; therefore, $\Delta P_{cap\ (pearl)} < \Delta P_{cap\ (chain)}$. However, before slipping occurs, the microchannel is completely filled with aqueous solution; thus, the aqueous solution cannot flow and break at the "chain" section, even with the difference in capillary pressure (Fig. 2B). After slipping, the expansion channel containing lubricating oil on the other plate is brought into contact with the chain-of-pearls channel (Fig. 2C). The capillary pressure after slipping at the pearl, $\Delta P_{cap\ (pearl)}$', and at the chain section, $\Delta P_{cap\ (chain)}$', can be described as follows:

$$\Delta P_{cap(pearl)'} \sim \left(\frac{1}{R}+\frac{1}{d_1+d_3}\right)\gamma\ \cos\theta \tag{4}$$

$$\Delta P_{cap(chain)'} \sim \left(\frac{1}{w}+\frac{1}{d_2+d_3}\right)\gamma\ \cos\theta \tag{5}$$

After slipping occurs, $\Delta P_{cap\ (pearl)}' < \Delta P_{cap\ (chain)}'$, and additional space is provided by the expansion channel; therefore, the aqueous solution flows from the chain to the pearl, and the aqueous solution self-partitions into droplets surrounded by a lubricating oil phase. The driving force of this spontaneous flow can be described as the difference in the capillary pressures:

$$\Delta P'_{cap(chain)} - \Delta P_{cap(pearl)'} \sim \left(\left(\frac{1}{w}+\frac{1}{d_2+d_3}\right)-\left(\frac{1}{R}+\frac{1}{d_1+d_3}\right)\right)\gamma\ \cos\theta \tag{6}$$

To reduce the loading flow resistance and to increase the consistency of the self-partitioning process, we also implemented butterfly bridging channels to provide a gradual change in the channel width. The butterfly channel shares the same depth (d_2) as the chain channel and is designed to widen from the middle (the angle is α) and be tangent to the pearl microwell (Fig. 2A). This butterfly channel can assist the splitting of aqueous fluid and cause the droplets formed by self-partitioning to be uniform.

A series of sp-SlipChip devices were designed and utilized for the generation of droplets of different sizes. Pearl microwells with diameters of 800 μm and depths of 75 μm, diameters of 450 μm and depths of 75 μm, diameters of 300 μm and depths of 75 μm, and diameters of 180 μm and depths of 45 μm were characterized by slip-induced droplet formation(Fig. 3A–D). The angle of the butterfly channel α is 53°. An aqueous solution containing food dye and fluorescein was used in these experiments, and the area of the droplet cross-section was measured. Droplets of all four sizes demonstrated very good uniformity with small standard deviations of 1.36% (n = 68), 1.78% (n = 240), 3.19% (n = 320), and 2.97% (n = 400), respectively (Fig. 3E–H).

The sp-SlipChip device was applied for the quantification of HPV-16 and HPV-18 viral DNA by digital LAMP. Based on the same mechanism of droplet formation, we designed a sp-SlipChip that can analyze both HPV-16 and HPV-18. For each sample, 2240 droplets of 4.5 nL each were generated, which corresponded to approximately 10 μL of total volume, and a total of 4480 droplets were generated on this device (Fig. 4A, Fig. S4). We characterized digital LAMP on this sp-SlipChip by the quantification of HPV-16 plasmid DNA. Solution containing LAMP master mix, primers, bovine serum albumin (BSA), and HPV plasmid DNA at serially diluted concentrations was introduced into the chain-of-pearls channels (experimental details in Supporting Information). After the loading was completed, the top plate was slipped down relative to the bottom plate to bring the chain-of-pearls channel on the bottom plate into contact with the expansion channel on the top plate. The aqueous solution in the channel self-partitioned into individual droplets. Then, the device was placed on a flat top thermal block at 65 °C for 60 min for LAMP. There was no significant increase in fluorescence intensity in the no-template control (NTC) experiments. Droplets containing target nucleic acids presented a significant increase in fluorescence intensity compared to the fluorescence intensity before incubation (Fig. 4B–E). The droplets adjacent to a positive droplet did not exhibit a significant increase in fluorescence intensity, which indicated that there was no cross-contamination between droplets.

We characterized the performance of digital LAMP on this sp-SlipChip with serially diluted HPV-16 plasmid DNA. Digital fluorescence patterns were obtained, and the number of positive wells increased proportionally with the concentration of the target template (Fig. 5A–D). The concentration of the target template determined from digital LAMP with a sp-SlipChip was analyzed with Poisson statistics (Kreutz et al., 2011), and the calculated concentration was in excellent agreement with the dilution ratio for HPV-16 plasmid DNA (Fig. 5E).

Furthermore, we tested this sp-SlipChip for the detection and quantification of HPV-16 and HPV-18 with nucleic acids extracted from clinical swab samples (Fig. 5F). In total, fifteen anonymous clinical samples were obtained from the International Peace Maternity & Child Health Hospital. The eluents of the clinical swab samples were divided into two halves. The first half was analyzed with the Roche Cobas 4800 HPV test in the hospital; seven samples were determined to be HPV-16 positive, five samples were determined to be HPV-18 positive, and three samples were determined to be negative. The nucleic acids extracted from the second half of the sample were analyzed by using digital LAMP on the sp-SlipChip. The sp-SlipChip method correctly identified both the seven HPV-16-positive samples (Fig. 5F, Patient ID

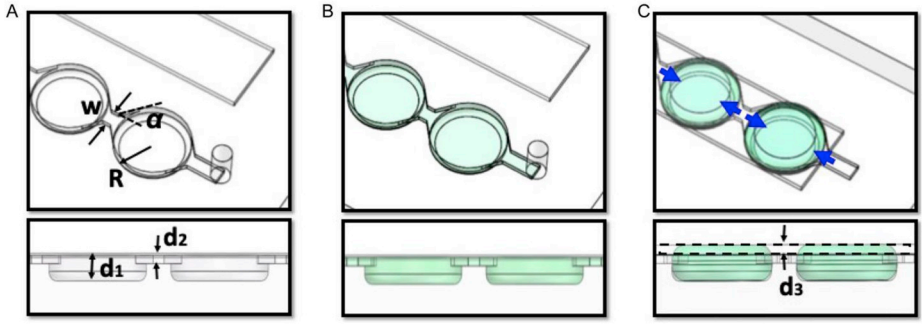

Fig. 2. Schematic drawing presenting the mechanism for slip-induced droplet formation. A) The assembled sp-SlipChip, where w represents the width of the chain channel; R represents the radius of the pearl microwell; α represents the angle of the butterfly connecting channel; d1 indicates the depth of the pearl microwell; and d2 indicates the depth of the chain channel. B) The chain-of-pearls channel is filled with green aqueous solution. C) After slipping occurs, the chain-of-pearls channel overlaps with the expansion channel, and the aqueous solution self-partitions to form individual droplets; d3 indicates the depth of the expansion channel. (For interpretation of the references to colour in this figure legend, the reader is referred to the Web version of this article.)

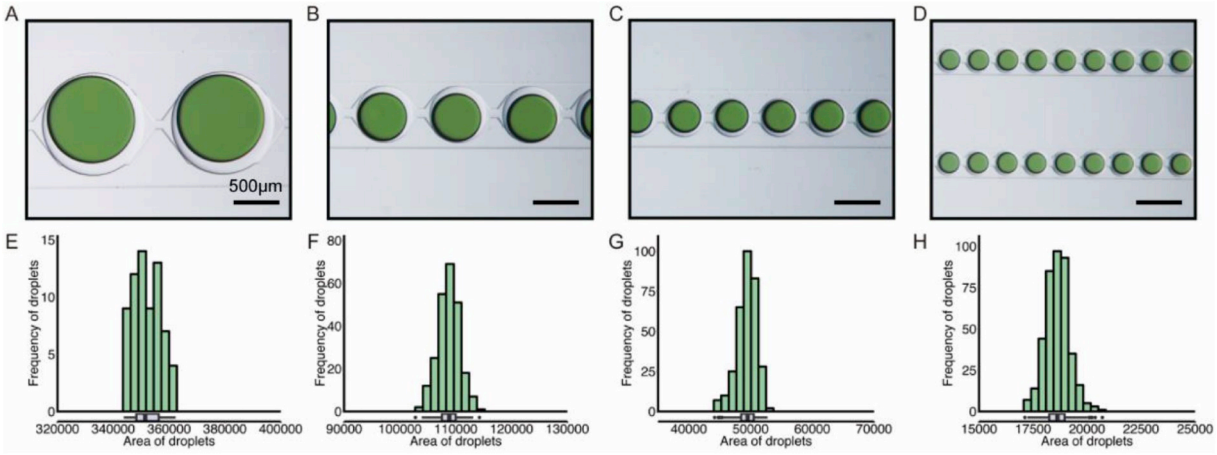

Fig. 3. Characterization of droplets of different sizes generated by the sp-SlipChip. A, E) The diameter of the pearl microwell is 800 μm n = 68. B, F) The diameter of the pearl microwell is 450 μm n = 240. C, G) The diameter of the pearl microwell is 300 μm n = 320. D, H) The diameter of the pearl microwell is 180 μm n = 400.

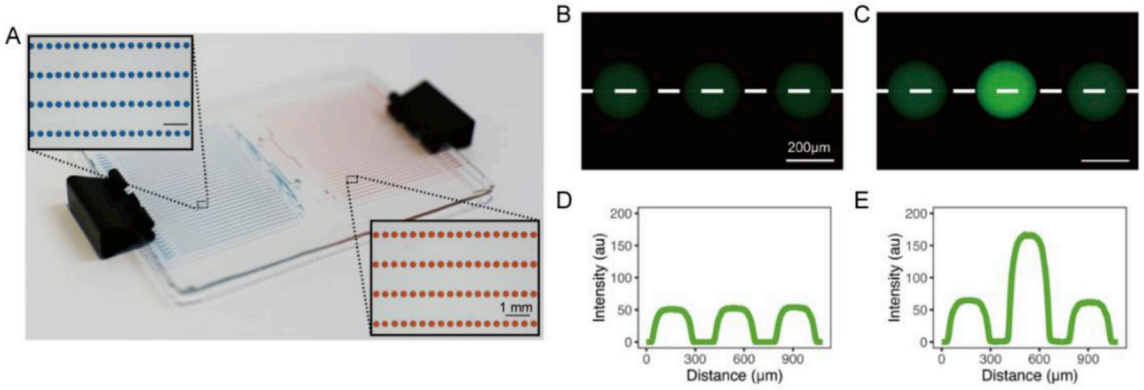

Fig. 4. Digital LAMP of HPV-16 plasmid DNA on a sp-SlipChip. (A) A bright-field photo of a sp-SlipChip loaded with aqueous solution spiked with blue and red food dye. (B) Fluorescence microphotograph showing part of the sp-SlipChip before incubation. (C) Fluorescence microphotograph acquired at the same position after thermal cycling: only the center well shows a significant increase in fluorescence from background levels. (D–E) A linescan presents the fluorescence intensity along the white dashed line. (For interpretation of the references to colour in this figure legend, the reader is referred to the Web version of this article.)

1–7) and the five HPV-18-positive samples (Fig. 5F, Patient ID 8–12) with viral loads ranging from 7.0×10^2 copies/mL to 1.4×10^7 copies/mL. The sp-SlipChip identified three samples as negative, which was in agreement with the Roche test method. The sp-SlipChip also identified three cases of HPV-16 and HPV-18 coinfection (Fig. 5F, Patient ID 3, 8, 11). Multiple infections with different types of HPV are common in infected subjects regardless of race and region(Muñoz et al., 2003; Wang et al., 2015). Multiplex PCR in one reaction, the core technique used by Cobas, may limit the sensitivity for the detection of multiple infections, resulting in underestimation of the prevalence of multiple infections (Wang et al., 2015; Zubach et al., 2012).

This sp-SlipChip-based mechanism can generate droplets with a slip-induced self-partitioning process, and it does not require the precise alignment of microwells on the contacting microfluidic plate or any additional control instrumentation, which greatly simplifies the assembly and operation of the device. Compared to traditional SlipChip approaches, this sp-SlipChip utilized continuous microchannels instead of distinct microwells at high density, and it could potentially be manufactured by large-scale manufacturing methods, such as injection molding, with less stringent requirements than other devices. The current version of the sp-SlipChip may have limitations for complex multistep fluidic manipulation; therefore, further development can be implemented to address the needs of specific applications.

The droplets generated by the sp-SlipChip were physically isolated, thereby reducing the volume of surfactant required for droplet formation and the complication of droplet coalescence during droplet manipulation, such as thermal cycling. The droplets in the sp-SlipChip are surrounded by a lubricating oil phase so that they can avoid contacting the solid surface to prevent the nonspecific adsorption of biomolecules to the solid surface. Moreover, the device tracks the position of each droplet, which could be highly informative for the serial interrogation of droplets, such as that performed in single-cell study and real time quantitative nucleic acid analysis.

The sp-SlipChip is also capable of generating droplets of different sizes on the sample device, which has been demonstrated previously on a multivolume SlipChip device for digital nucleic acid quantification over a large dynamic range(Shen et al., 2011b). Furthermore, this device can also be potentially implemented with multistep operations for the parallel manipulation of droplets with high throughput.

The dimensions of the chain section of the chain-of-pearls channel have a significant impact on the capillary pressure and the fluidic loading pressure. Reducing the cross-section of the chain section increases the difference in capillary pressure and facilitates the breaking of aqueous solution and the formation of droplets. However, reducing the cross-section of the chain section also increases the flow resistance of the chain-of-pearls channel and the difficulty of loading aqueous solution into the sp-SlipChip. Therefore, it is important to balance the capillary pressure effect and the flow resistance of the entire device during the device design.

This sp-SlipChip can handle patient samples and provide an accurate

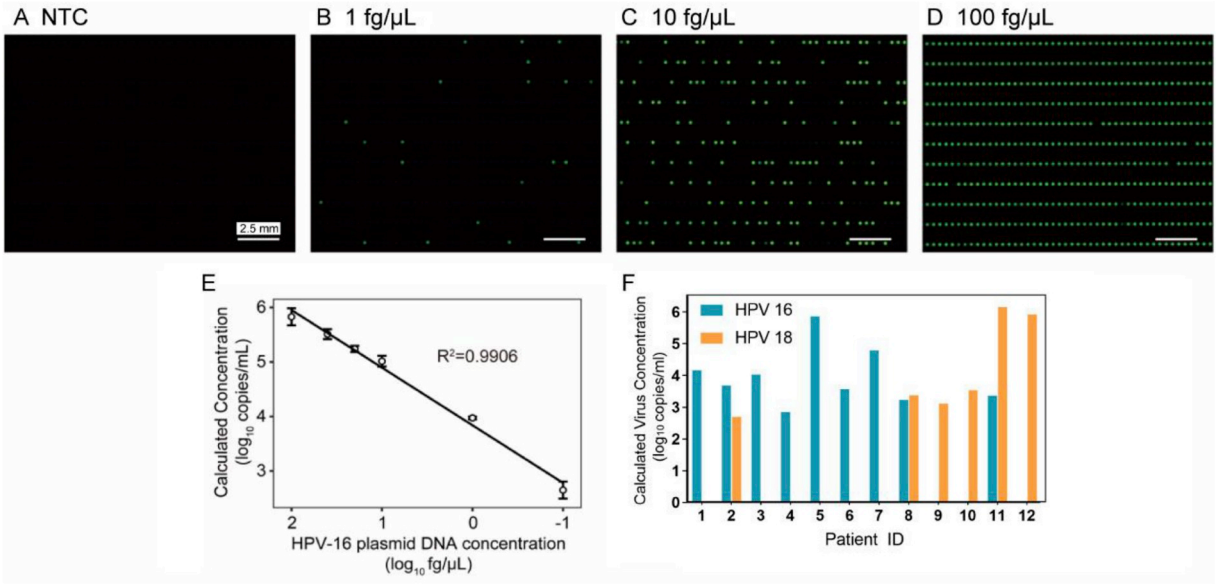

Fig. 5. Digital LAMP for the quantification of HPV viral load on a sp-SlipChip. (A) A representative fluorescence image of a sp-SlipChip with a no-template control (NTC). (B) Representative fluorescence images of digital LAMP for the quantification of HPV-16 plasmid DNA at 1 fg/μL. (C) Representative fluorescence images of digital LAMP for the quantification of HPV-16 plasmid DNA at 10 fg/μL. (D) Representative fluorescence images of digital LAMP for the quantification of HPV-16 plasmid DNA at 100 fg/μL. (E) Plots of HPV-16 plasmid DNA concentrations versus calculated concentrations from a linear regression for the quantification of HPV-16 plasmid DNA. n = 3, and error bars represent the standard deviation. (F) Quantification of HPV-16 and HPV-18 viral loads with nucleic acid extracted from anonymous clinical cervical swab samples.

digital LAMP quantification of viral load with simple manipulation steps. Both NAA and bacterial identification have been achieved with droplets of plasma or whole blood samples(Kang et al., 2014; Zhang et al., 2015b). Therefore, the sp-SlipChip can potentially enable digital nucleic acid quantification and cell analysis directly from physiologically relevant body fluids. Furthermore, the sp-SlipChip might be seamlessly integrated with on-chip sample preparation methods (Mahalanabis et al., 2009; Schlappi et al., 2016) as well as with easy readout methods (Rodriguez-Manzano et al., 2016) for sample-in-answer-out total analysis in resource-limited settings.

4. Conclusion

In this paper, we have demonstrated a sp-SlipChip device for the generation of droplets with very good uniformity and robustness. Digital LAMP can be used with this sp-SlipChip to perform quantitative analysis of HPV-16/18 nucleic acids extracted from clinical swab samples. No cross-contamination was observed between adjacent droplets during amplification. This sp-SlipChip does not require the precise alignment of microfeatures on the contacting plate, which makes it a promising tool for chemical and biological research in laboratories and potentially in clinical medical diagnostic applications, especially in resource-limited settings.

Declaration of competing interest

The authors declare that they have no known competing financial interests or personal relationships that could have appeared to influence the work reported in this paper.

CRediT authorship contribution statement

Ziqing Yu: Investigation, Formal analysis, Writing - original draft. **Weiyuan Lyu:** Investigation, Formal analysis, Writing - original draft. **Mengchao Yu:** Investigation, Formal analysis, Writing - original draft. **Qian Wang:** Formal analysis, Resources, Writing - original draft. **Haijun Qu:** Investigation, Formal analysis. **Rustem F. Ismagilov:** Conceptualization. **Xu Han:** Writing - review & editing. **Dongmei Lai:** Investigation, Resources, Writing - review & editing. **Feng Shen:** Conceptualization, Funding acquisition, Methodology, Writing - original draft.

Acknowledgments

We thank Dr. Rebecca R. Pompano and Ms. Jing Ling for editing the manuscript. This work is supported by the National Natural Science Foundation of China (no. 21705109), the Innovation Research Plan supported by Shanghai Municipal Education Commission (no. ZXWF082101), the Natural Science Foundation of Shanghai (no. 19ZR1475900), the interdisciplinary program of Shanghai Jiao Tong University (no. YG2015ZD11), and supported by Shanghai Jiao Tong University Scientific and Technological Innovation Funds.

Appendix A. Supplementary data

Supplementary data to this article can be found online at https://doi.org/10.1016/j.bios.2020.112107.

References

Bai, Y., Qu, Y., Wu, Z., Ren, Y., Cheng, Z., Lu, Y., Hu, J., Lou, J., Zhao, J., Chen, C., Mao, H., 2019. Absolute quantification and analysis of extracellular vesicle lncRNAs from the peripheral blood of patients with lung cancer based on multi-colour fluorescence chip-based digital PCR. Biosens. Bioelectron. 142, 111523. https://doi.org/10.1016/j.bios.2019.111523.

Cai, D., Xiao, M., Xu, P., Xu, Y.C., Du, W., 2014. An integrated microfluidic device utilizing dielectrophoresis and multiplex array PCR for point-of-care detection of pathogens. Lab Chip Miniaturisation Chem. Biol. 14, 3917–3924. https://doi.org/10.1039/c4lc00669k.

Cao, L., Cui, X., Hu, J., Li, Z., Choi, J.R., Yang, Q., Lin, M., Hui, L.Y., Xu, F., 2016. Advances in digital polymerase chain reaction (dPCR) and its emerging biomedical applications. Biosens. Bioelectron. 1–15 https://doi.org/10.1016/j.bios.2016.09.082.

Chen, Z., Liao, P., Zhang, F., Jiang, M., Zhu, Y., Huang, Y., 2017. Centrifugal microchannel array droplet generation for highly parallel digital PCR. Lab Chip 17, 235–240. https://doi.org/10.1039/C6LC01305H.

Crow, J.M., 2012. HPV: the global burden. Nature 488, S2–S3. https://doi.org/10.1038/488S2a.

De Martel, C., Ferlay, J., Franceschi, S., Vignat, J., Bray, F., Forman, D., Plummer, M., 2012. Global burden of cancers attributable to infections in 2008: a review and synthetic analysis. Lancet Oncol. 13, 607–615. https://doi.org/10.1016/S1470-2045(12)70137-7.

Du, W., Li, L., Nichols, K.P., Ismagilov, R.F., 2009. SlipChip. Lab Chip 9, 2286–2292. https://doi.org/10.1039/b908978k.

Heyries, K.A., Tropini, C., Vaninsberghe, M., Doolin, C., Petriv, O.I., Singhal, A., Leung, K., Hughesman, C.B., Hansen, C.L., 2011. Megapixel digital PCR. Nat. Methods 8, 649–651. https://doi.org/10.1038/nmeth.1640.

Hindson, B.J., Ness, K.D., Masquelier, D.A., Belgrader, P., Heredia, N.J., Makarewicz, A. J., Bright, I.J., Lucero, M.Y., Hiddessen, A.L., Legler, T.C., Kitano, T.K., Hodel, M.R., Petersen, J.F., Wyatt, P.W., Steenblock, E.R., Shah, P.H., Bousse, L.J., Troup, C.B., Mellen, J.C., Wittmann, D.K., Erndt, N.G., Cauley, T.H., Koehler, R.T., So, A.P., Dube, S., Rose, K.A., Montesclaros, L., Wang, S., Stumbo, D.P., Hodges, S.P., Romine, S., Milanovich, F.P., White, H.E., Regan, J.F., Karlin-Neumann, G.A., Hindson, C.M., Saxonov, S., Colston, B.W., 2011. High-throughput droplet digital PCR system for absolute quantitation of DNA copy number. Anal. Chem. 83, 8604–8610. https://doi.org/10.1021/ac202028g.

Huang, J.T., Liu, Y.J., Wang, J., Xu, Z.G., Yang, Y., Shen, F., Liu, X.H., Zhou, X., Liu, S.M., 2015. Next generation digital PCR measurement of hepatitis B virus copy number in formalin-fixed paraffin-embedded hepatocellular carcinoma tissue. Clin. Chem. 61, 290–296. https://doi.org/10.1373/clinchem.2014.230227.

Jiang, C.-Y., Zhao, J.-K., Shen, C., Qiao, Y., Liu, S.-J., Du, W., Dong, L., Hu, X., Zhang, X., Wang, Y., Ismagilov, R.F., 2016. High-throughput single-cell cultivation on microfluidic streak plates. Appl. Environ. Microbiol. 82, 2210–2218. https://doi.org/10.1128/AEM.03588-15.

Kang, D.-K., Ali, M.M., Zhang, K., Huang, S.S., Peterson, E., Digman, M. a, Gratton, E., Zhao, W., 2014. Rapid detection of single bacteria in unprocessed blood using Integrated Comprehensive Droplet Digital Detection. Nat. Commun. 5, 5427. https://doi.org/10.1038/ncomms6427.

Kreutz, J.E., Munson, T., Huynh, T., Shen, F., Du, W., Ismagilov, R.F., 2011. Theoretical design and analysis of multivolume digital assays with wide dynamic range validated experimentally with microfluidic digital PCR. Anal. Chem. 83, 8158–8168. https://doi.org/10.1021/ja2060116.

Kreutz, J.E., Wang, J., Sheen, A.M., Thompson, A.M., Staheli, J.P., Dyen, M.R., Feng, Q., Chiu, D.T., 2019. Self-digitization chip for quantitative detection of human papillomavirus gene using digital LAMP. Lab Chip 19, 1035–1040. https://doi.org/10.1039/c8lc01223g.

Li, L., Du, W., Ismagilov, R., 2010. User-loaded SlipChip for equipment-free multiplexed nanoliter-scale experiments. J. Am. Chem. Soc. 132, 106–111. https://doi.org/10.1021/ja908555n.

Liu, W., Chen, D., Du, W., Nichols, K.P., Ismagilov, R.F., 2010. SlipChip for Immunoassays in Nanoliter Volumes, vol. 82, pp. 14613–14619.

Lo, Y.M.D., Lun, F.M.F., Chan, K.C.A., Tsui, N.B.Y., Chong, K.C., Lau, T.K., Leung, T.Y., Zee, B.C.Y., Cantor, C.R., Chiu, R.W.K., 2007. Digital PCR for the molecular detection of fetal chromosomal aneuploidy. Proc. Natl. Acad. Sci. Unit. States Am. 104, 13116–13121. https://doi.org/10.1073/pnas.0705765104.

Luo, L., Nie, K., Yang, M.J., Wang, M., Li, J., Zhang, C., Liu, H.T., Ma, X.J., 2011. Visual detection of high-risk human papillomavirus genotypes 16, 18, 45, 52, and 58 by loop-mediated isothermal amplification with hydroxynaphthol blue dye. J. Clin. Microbiol. 49, 3545–3550. https://doi.org/10.1128/JCM.00930-11.

Mahalanabis, M., Al-Muayad, H., Kulinski, M.D., Altman, D., Klapperich, C.M., 2009. Cell lysis and DNA extraction of gram-positive and gram-negative bacteria from whole blood in a disposable microfluidic chip. Lab Chip 9, 2811–2817. https://doi.org/10.1039/b905065p.

Muñoz, N., Bosch, F.X., de Sanjosé, S., Herrero, R., Castellsagué, X., Shah, K.V., Snijders, P.J.F., Meijer, C.J.L.M., 2003. Epidemiologic classification of human papillomavirus types associated with cervical cancer. N. Engl. J. Med. 348, 518–527. https://doi.org/10.1056/NEJMoa021641.

Nie, M., Zheng, M., Li, C., Shen, F., Liu, M., Luo, H., Song, X., Lan, Y., Pan, J.Z., Du, W., 2019. Assembled step emulsification device for multiplex droplet digital polymerase chain reaction. Anal. Chem. 91, 1779–1784. https://doi.org/10.1021/acs.analchem.8b04313.

Ottesen, E. a, Hong, J.W., Quake, S.R., Leadbetter, J.R., 2006. Microfluidic digital PCR enables multigene analysis of individual environmental bacteria. Science 314, 1464–1467. https://doi.org/10.1126/science.1131370.

Park, Y., Lee, E., Choi, J., Jeong, S., Kim, H.S., 2012. Comparison of the abbott realtime high-risk human papillomavirus (HPV), roche cobas HPV, and hybrid capture 2 assays to direct sequencing and genotyping of HPV DNA. J. Clin. Microbiol. 50, 2359–2365. https://doi.org/10.1128/JCM.00337-12.

Pompano, R.R., Platt, C.E., Karymov, M.A., Ismagilov, R.F., 2012. Control of initiation, rate, and routing of spontaneous capillary-driven flow of liquid droplets through microfluidic channels on slipchip. Langmuir 28, 1931–1941. https://doi.org/10.1021/la204399m.

Rodriguez-Manzano, J., Karymov, M.A., Begolo, S., Selck, D.A., Zhukov, D.V., Jue, E., Ismagilov, R.F., 2016. Reading out single-molecule digital RNA and DNA isothermal amplification in nanoliter volumes with unmodified camera phones. ACS Nano 10, 3102–3113. https://doi.org/10.1021/acsnano.5b07338.

Schlappi, T.S., McCalla, S.E., Schoepp, N.G., Ismagilov, R.F., 2016. Flow-through capture and in situ amplification can enable rapid detection of a few single molecules of nucleic acids from several milliliters of solution. Anal. Chem. 88, 7647–7653. https://doi.org/10.1021/acs.analchem.6b01485.

Seoud, M., Tjalma, W.A.A., Ronsse, V., 2011. Cervical adenocarcinoma: moving towards better prevention. Vaccine 29, 9148–9158. https://doi.org/10.1016/j.vaccine.2011.09.115.

Shen, C., Xu, P., Huang, Z., Cai, D., Liu, S.J., Du, W., 2014. Bacterial chemotaxis on SlipChip. Lab Chip 14, 3074–3080. https://doi.org/10.1039/c4lc00213j.

Shen, F., Davydova, E.K., Du, W., Kreutz, J.E., Piepenburg, O., Ismagilov, R.F., 2011a. Digital isothermal quantification of nucleic acids via simultaneous chemical initiation of recombinase polymerase amplification reactions on SlipChip. Anal. Chem. 83, 3533–3540. https://doi.org/10.1021/ac200247e.

Shen, F., Du, W., Kreutz, J.E., Fok, A., Ismagilov, R.F., 2010. Digital PCR on a SlipChip. Lab Chip 10, 2666–2672. https://doi.org/10.1039/c004521g.

Shen, F., Sun, B., Kreutz, J.E., Davydova, E.K., Du, W., Reddy, P.L., Joseph, L.J., Ismagilov, R.F., 2011b. Multiplexed quantification of nucleic acids with large dynamic range using multivolume digital RT-PCR on a rotational SlipChip tested with HIV and hepatitis C viral load. J. Am. Chem. Soc. 133, 17705–17712. https://doi.org/10.1021/ja2060116.

Sun, B., Shen, F., McCalla, S.E., Kreutz, J.E., Karymov, M.a., Ismagilov, R.F., 2013. Mechanistic evaluation of the pros and cons of digital RT-LAMP for HIV-1 viral load quantification on a microfluidic device and improved efficiency via a two-step digital protocol. Anal. Chem. 85, 1540–1546. https://doi.org/10.1021/ac3037206.

Taly, V., Pekin, D., Benhaim, L., Kotsopoulos, S.K., Corre, D. Le, Li, X., Atochin, I., Link, D.R., Griffiths, A.D., Pallier, K., Blons, H., Bouché, O., Landi, B., Hutchison, J. B., Laurent-Puig, P., 2013. Multiplex picodroplet digital PCR to detect KRAS mutations in circulating DNA from the plasma of colorectal cancer patients. Clin. Chem. 59, 1722–1731. https://doi.org/10.1373/clinchem.2013.206359.

Wang, R., Guo, X. lei, Wisman, G.B.A., Schuuring, E., Wang, W. feng, Zeng, Z. yu, Zhu, H., Wu, S. wei, 2015. Nationwide prevalence of human papillomavirus infection and viral genotype distribution in 37 cities in China. BMC Infect. Dis. 15, 1–10. https://doi.org/10.1186/s12879-015-0998-5.

Wu, Z., Bai, Y., Cheng, Z., Liu, F., Wang, P., Yang, D., Li, G., Jin, Q., Mao, H., Zhao, J., 2017. Absolute quantification of DNA methylation using microfluidic chip-based digital PCR. Biosens. Bioelectron. 96, 339–344. https://doi.org/10.1016/j.bios.2017.05.021.

Yu, M., Chen, X., Qu, H., Ma, L., Xu, L., Lv, W., Wang, H., Ismagilov, R.F., Li, M., Shen, F., 2019. Multistep SlipChip for the generation of serial dilution nanoliter arrays and hepatitis B viral load quantification by digital loop mediated isothermal amplification. Anal. Chem. 91, 8751–8755. https://doi.org/10.1021/acs.analchem.9b01270.

Zeng, Y., Shin, M., Wang, T., 2013. Programmable active droplet generation enabled by integrated pneumatic micropumps. Lab Chip 13, 267–273. https://doi.org/10.1039/c2lc40906b.

Zhang, K., Kang, D.-K., Ali, M.M., Liu, L., Labanieh, L., Lu, M., Riazifar, H., Nguyen, T.N., Zell, J.a., Digman, M.a., Gratton, E., Li, J., Zhao, W., 2015a. Digital quantification of miRNA directly in plasma using integrated comprehensive droplet digital detection. Lab Chip. https://doi.org/10.1039/C5LC00650C.

Zhang, K., Kang, D.K., Ali, M.M., Liu, L., Labanieh, L., Lu, M., Riazifar, H., Nguyen, T.N., Zell, J.A., Digman, M.A., Gratton, E., Li, J., Zhao, W., 2015b. Digital quantification of miRNA directly in plasma using integrated comprehensive droplet digital detection. Lab Chip 15, 4217–4226. https://doi.org/10.1039/c5lc00650c.

Zhou, S., Gou, T., Hu, J., Wu, W., Ding, X., Fang, W., Hu, Z., Mu, Y., 2019. A highly integrated real-time digital PCR device for accurate DNA quantitative analysis. Biosens. Bioelectron. 128, 151–158. https://doi.org/10.1016/j.bios.2018.12.055.

Zhu, P., Wang, L., 2017. Passive and active droplet generation with microfluidics: a review. Lab Chip 17, 34–75. https://doi.org/10.1039/C6LC01018K.

Zhu, Y., Zhang, Y.X., Liu, W.W., Ma, Y., Fang, Q., Yao, B., 2015. Printing 2-dimensional droplet array for single-cell reverse transcription quantitative PCR assay with a microfluidic robot. Sci. Rep. 5, 1–7. https://doi.org/10.1038/srep09551.

Zubach, V., Smart, G., Ratnam, S., Severini, A., 2012. Novel microsphere-based method for detection and typing of 46 mucosal human papillomavirus types. J. Clin. Microbiol. 50, 460–464. https://doi.org/10.1128/JCM.06090-11.